Biophysical basis for brain folding and misfolding patterns in ferrets and humans

Gary P. T. Choi[1], Chunzi Liu[2], Sifan Yin[2], Gabrielle Séjourné[2,3], Richard S. Smith[4], Christopher A. Walsh[5,6], L. Mahadevan[2,7*]

[1]Department of Mathematics, The Chinese University of Hong Kong, Hong Kong

[2]School of Engineering and Applied Sciences, Harvard University, Cambridge, MA, USA

[3]Department of Cell Biology, Duke University, Durham, NC, USA

[4]Department of Pharmacology, Feinberg School of Medicine, Northwestern University, Chicago, IL, USA

[5]Departments of Neurology and Pediatrics, Harvard Medical School, Boston, MA, USA

[6]Division of Genetics and Genomics, Manton Center for Orphan Disease, and Howard Hughes Medical Institute, Boston Children's Hospital, Boston, MA, USA

[7]Departments of Physics, and Organismic and Evolutionary Biology, Harvard University, Cambridge, MA, USA

*To whom correspondence should be addressed; E-mail: lmahadev@g.harvard.edu

A mechanistic understanding of neurodevelopment requires us to follow the multiscale processes that connect molecular genetic processes to macroscopic cerebral cortical formations and thence to neurological function. Using magnetic resonance imaging of the brain of the ferret, a model organism for studying cortical morphogenesis, we create *in vitro* physical gel models and *in silico* numerical simulations of normal brain gyrification. Using observations of genetically manipulated animal models, we identify cerebral cortical thickness and cortical expansion rate as the primary drivers of dysmorphogenesis and demonstrate that *in silico* models allow us to examine the causes of aberrations in morphology and developmental processes at various stages of cortical

ontogenesis. Finally, we explain analogous cortical malformations in human brains, with comparisons with human phenotypes induced by the same genetic defects, providing a unified perspective on brain morphogenesis that is driven proximally by genetic causes and affected mechanically via variations in the geometry of the brain and differential growth of the cortex.

Understanding the growth and form of normal and abnormal cortical convolutions (gyri and sulci) is important for the study of human neurodevelopmental diseases (*1–5*). During early brain development, the cortical plate expands tangentially relative to the underlying white matter (*6*). This pattern of growth is the central cause of gyrification; indeed tangential cortical expansion creates compressive forces on the faster-growing outer layer of the cortex and tensile forces on the attached slower-growing inner layer, and the relative-growth induced forces cause cortical folding as suggested more than a century ago (*7*) and first quantitatively elucidated nearly fifty years ago (*8*). At a molecular and cellular level, neurogenesis, neuronal migration, and neuronal differentiation all contribute to the tangential growth of the developing cortex via processes such as an increase in either the number or size of cells (*9–12*). Recent models that take these facts into account attempt to explain gyrification in terms of a simple mechanical instability, termed sulcification (*13*), that when iterated with variations (*14*) shows that tangential expansion of the gray matter constrained by the white matter can explain a range of different morphologies seen in the brains of different organisms (*15, 16*). Furthermore, when deployed over developmental time to simulate normal human cortical convolution, the results can capture a substantial range of features seen in normal human fetal brain morphogenesis (*17*). However, these and other similar studies (*18–29*) do not allow us to understand malformations of cortical development (MCD) owing to our inability to probe the development of the human fetal brain *in utero*.

An alternative strategy is to turn to model organisms to study the developmental trajectory of MCDs. Since commonly used animal models such as the mouse and rat have lissencephalic

cortices, the ferret, a gyrencephalic non-primate, has been favored as an experimentally tractable laboratory organism that demonstrates cortical folding patterns that are roughly similar to that observed in the human (*9, 30–33*). Furthermore, since the process of cortical folding in the ferret is almost exclusively postnatal, with the progressive development of cortical gyri and sulci from postnatal day 0 (P0) to adolescence (Fig. 1), it is more easily observable. Finally, the ability to perform region-specific genetic manipulation of the ferret brain through *in utero* electroporation (*34, 35*) makes the ferret an ideal system for modeling normal and abnormal neurodevelopmental processes.

Inspired by our previous studies using physical experiments with swelling gels and computational models of brain growth (*15, 17, 36*), we model the folding of a normal ferret brain using a physical gel model and a computational model based on the principle of constrained cortical expansion and compare the simulation results with the real brain development using various geometric morphometric approaches. We then use the computational and physical models to reproduce defective developmental processes of the ferret brain and show that they are consistent with biological experiments that manipulate different molecular drivers of neurogenesis, neuronal migration and cell growth in the cortex that underlie its relative thickness and expansion rate. Taken together, our studies provide a mesoscopic approach to brain morphogenesis that combines computational *in silico* and physical gel *in vitro* models with morphological and molecular analysis of ferret cortical disease models, and shed light on analogous MCDs in human brains.

Physical gel model

Inspired by the observation that soft physical gels swell and fold superficially when immersed in solvents, we constructed a physical simulacrum of ferret brain folding following our previous protocols (*15, 17*). Specifically, we produced two-layer PDMS gel models of the ferret brain at various ages based on surfaces reconstructed from MR Images (see SI Section S1 for details).

We then immersed the two-layer gel brain model in n-hexane, which led to folding patterns by solvent-driven swelling of the outer layers (Fig. 2**a**).

Fig. 2**b** shows the experimental results for a P8 gel brain; it swells nonuniformly and folds progressively from an initial state that has invaginations corresponding to the cruciate sulcus (crs), the coronal sulcus (cns), and the suprasylvian sulcus (sss). The post-swelling state shows the development of sulci corresponding in location and self-contacting nature to the crs, cns, sss, and the formation of rhinal sulcus (rs), the pseudosylvian sulcus (pss), and lateral sulcus (ls), and ansate sulcus (as) observed in real ferrets aged P21 and older. Fig. 2**c** shows another swelling experiment with a starting shape corresponding to the P16 gel brain, from which we observe a similar progression in the folding patterns. We see that our minimal physical model can capture the qualitative aspects of the folding transitions in the ferret brain (see also SI Section S1 and Video S1–S2).

Computational model

To complement our physical experiments with quantitative simulations of ferret brain development, we followed the approach in (*15, 17*) and considered a neo-Hookean material model for the brain cortex consisting of a layer of gray matter on top of a deep layer of white matter with volumetric strain energy density

$$W = \frac{\mu}{2}\left[Tr(\mathbf{F}\mathbf{F}^T)J^{-2/3} - 3\right] + \frac{K}{2}(J-1)^2, \tag{1}$$

where $\mathbf{F}$ is the deformation gradient, $J = \det(\mathbf{F})$, μ is the shear modulus and K is the bulk modulus. We assume that $K = 5\mu$ for a modestly compressible material. Computer simulations were then performed on tetrahedral meshes of ferret brains to model the gyrification (see SI Section S2 for more details).

We considered both simulations that modeled the changes in brain morphology from P0 to

P32 as one continuous process (Fig. 3**a**, see also SI Movie S3) and stepwise simulations that considered the growth process in stages, i.e. from P0 to P4, from P4 to P8, from P8 to P16 and from P16 to P32 (Fig. 3**b**, see also SI Movie S4). In both sets of simulations, the emergence of cortical folding can be observed. In the continuous simulation approach, we observed the appearance of multiple minor folds since the continuous simulations only depend on the P0 initial brain, so that the effect of minor features in the P0 brain on the brain growth may accumulate over time. By contrast, in the stepwise simulation approach which focuses on multiple shorter growth periods, and thus reduces the accumulation of shape variations over time. Comparing the P16 results of stepwise numerical simulation, the gel experiment and the P16 real brain, we observe that the folding patterns are visually very similar (Fig. 4**a**). For a more quantitative comparison, we applied a method based on aligning landmarks using spherical mapping termed FLASH (Fast Landmark Aligned Spherical Harmonic Parameterization) (*37*) to parameterize the simulated P16 ferret brain and the P16 brain surface generated from the MRI scans onto the unit sphere using landmark-aligned optimized conformal mappings, with the coronal sulcus (cns), suprasylvian sulcus (sss), presylvian sulcus (prs), and pseudosylvian sulcus (pss) on both the left and right hemispheres used as landmarks (see Fig. 4**a**, and SI Section S3 for more details). We then assessed the geometric similarity of the two brain surfaces on the spherical domain in terms of their shape index (*38*), which is a surface measure defined based on the surface mean curvature and Gaussian curvature. The similarity of the two shape indices suggests that the folding pattern produced by our simulation is close to the actual folding pattern (see SI Section S3 and (*39*) for more details of the morphometric method). We further utilized spherical harmonic-based representations of the two brains, which also shows that the two brains have consistent geometric similarities (see SI Section S3).

Neurology of ferret and human cortical malformations

The effectiveness of our differential growth-based model in quantifying the normative development of normal ferret brains begs the question of whether we can use the same framework to study malformations of cortical development (MCD). For instance, *SCN3A* encodes a sodium channel and specific missense mutations of it are associated with the MCD polymicrogyria (PMG) (*40*), while genetic manipulations of *ASPM* have also been shown to produce severe microcephaly in human and ferret brains (*32*), while disrupting *TMEM161B* leads to cortical malformations in humans and ferrets (*41*). In these and other examples, various genetic causes lead to variations in the cortical thickness ratio h/R and/or the tangential growth ratio g in space and time, that we know to be critical geometric parameters that change the physical nature of the sulcification instability driving cortical folding.

In Fig. 5**a**, we show a control human brain MRI (top), a wild-type P16 ferret brain MRI (middle), and the stepwise numerical simulation result under the normal parameter setup (bottom). In Fig. 5**b**, (top) we show the MCD polymicrogyria (PMG) phenotype in humans associated with over-expression of a mutated *SCN3A* gene. In Fig. 5**b** (middle), we show that the same mutation in ferrets leads to an increased number of tightly packed folds in the perisylvian region. To model this cortical malformation, we performed a modified numerical simulation with the cortical thickness reduced to $1/4$ of the original thickness at a localized zone around the perisylvian region of the P8 brain model. From the modified numerical simulation result (Fig. 5**b**, bottom), we can see that our model can qualitatively capture perisylvian PMG.

In Fig. 5**c** (top) and Fig. 5**c** (middle) (*32*) we show that *ASPM* mutants produce severe microcephaly in human and ferret brains (*32*), because the cortical surface area is reduced while there is no significant change in the cortical thickness. To reproduce this malformation we consider a modified computational experiment with a reduction of the growth rate to $1/4$ of the

original rate. In Fig. 5**c** (bottom), we show the results of numerical simulations that lead to less prominent folding when compared to the normal brain, consistent with observations in human and ferret brains.

Finally, in Fig. 5**d** (top) and Fig. 5**d** (middle) (*41*), we show that disrupting *TMEM161B* also leads to cortical malformations in human and ferret brains, with shallower sulci. Modifying the morphogenetic simulations with a reduction of the growth rate to $3/4$ of the original rate and an increase of the cortical thickness to 1.5 times the original thickness leads to results shown in Fig. 5**d** (bottom) that matches the experimentally observed malformation patterns qualitatively.

In SI Section S4, we present additional physical gel and computational experiments to demonstrate the effect of different combinations of the growth rate and cortical thickness parameters on the cortical malformation results.

Discussion

Understanding the growth and form of the cerebral cortex is a fundamental question in neurobiology, and the experimentally accessible progressive postnatal development of the ferret brain makes it an ideal system for analysis. Here, we have used a combination of physical and computational models based on differential growth to show how ferret brain morphologies arise. By modifying the scaled cortical layer thickness and the tangential growth profile in our model, we have qualitatively reproduced various cortical malformations and shown how developmental mechanisms lead to morphological manifestations with potential functional implications. All together, our study elucidates the normal and abnormal folding in the ferret brain as a function of its genetic antecedents that lead to changes in the geometry of the cortex and thence to different physical folding patterns with functional consequences. A computational and physical-gel brain study informed by detailed MRI of ferret and human fetal brains allows us to move towards a synthesis of the genetic, physical and morphological basis for cortical malformations.

While this work has focused on the morphogenesis and dysmorphogenesis of the ferret brain, one may also use the physical and computational models to understand how folding occurs across organisms as in our complementary study (*39*), where we investigate how modifying the cortical layer thickness and the tangential growth rate would lead to abnormal folding in different species.

Methods

Physical gel model for ferret brain folding

Beginning with T2-weighted motion-corrected anatomical MR images of ferret brains of various ages (*42*), we recreated digital maps of the surfaces of pre-swelling brain states. Then, we followed our prior experimental approach (*15, 17*) and produced two-layer PDMS gel models of the ferret brain at various ages based on the reconstructed brain surfaces. Specifically, we first generated a negative rubber mold with Ecofl ex 00-30 from a 3D-printed brain plastic model and then the core gel with SYLGARD 184 at a 1:45 crosslinker:base ratio. To mimic the cortical layer, we surface-coated 4 layers of PDMS gel at a 1:35 crosslinker:base ratio onto the core layer. Finally, tangential cortical growth was mimicked by immersing the two-layer gel brain model in n-hexane for 1.5 hours, which resulted in solvent-driven swelling of the outer layers, leading to folding patterns. See SI Section S1 for details.

Computational model for ferret brain folding

Three geometrical parameters of the 3D brain models control its morphogenesis: the average brain size R (determined for example by its volume), the average cortical thickness T and the average tangential expansion ratio of the cortex relative to the white matter, g^2. To characterize brain development in the ferret, we followed the empirical scaling laws for gray-matter volume to thickness described in (*15*) and set $R/T \approx 10$ with the tangential expansion ratio $g \approx 1.9$,

along with an indicator function $\theta(y) = (1 + e^{10(y/T-1)})^{-1}$, with y the distance from surface in a material reference frame used to distinguish between the cortical gray matter layer (with $\theta = 1$) from the deeper white matter (with $\theta = 0$).

Using MRIs of ferret brains, we created a computational model of the initial brain size and shape, that was discretized using tetrahedral meshes with over one million tetrahedral elements using Netgen (*43*). Using a finite element method implemented using a discretized version of the energy of the system (1), we minimized the energy by quasistatic equilibration using an explicit solver (*17*), while growth was applied incrementally using the form described earlier by expanding the tetrahedral elements with inversion handling (*44*) and a nodal pressure formulation (*45*). Self-avoidance of the surface was handled using the penalty-based vertex-triangle contact processing (*46*). We also enforce the condition that there is no growth in the central part as well as in the bottom part of the brain to better simulate the development of ferret brains. See SI Section S2 for more details.

Data availability

Newborn ferret brain surfaces will be made available upon request. All other data are included in the article and/or supplementary material.

Competing interests

The authors declare no conflict of interest.

Author contributions

L.M. conceived of the project and designed research. G.P.T.C. carried out the computations, C.L. and G.S. carried out the gel swelling experiments, S.Y. carried out the morphometric analysis,

R.S.S. and C.W. carried out the genetic mutation experiments. G.P.T.C. and L.M. wrote the paper with input from all authors, and all authors edited the paper.

Acknowledgments

We thank Jun Young Chung and James Weaver for their help with preliminary experiments. This work is supported in part by the Harvard Quantitative Biology Initiative and the NSF-Simons Center for Mathematical and Statistical Analysis of Biology at Harvard, award no. 1764269 (to G.P.T.C. and L.M.), the Simons Foundation and the Henri Seydoux Fund (to L.M.). G.P.T.C. is also supported by the CUHK Faculty of Science Direct Grant Direct Grant for Research (Project Code 4053650). C.A.W. is supported by the NINDS through R01NS032457 and R01NS035129, the Templeton Foundation, and by the Allen Discovery Center for Human Brain Evolution. C.A.W. is an Investigator of the Howard Hughes Medical Institute. R.S.S was supported by R00NS112604.

References

1. J. H. Lui, D. V. Hansen, and A. R. Kriegstein, "Development and evolution of the human neocortex," *Cell*, vol. 146, no. 1, pp. 18–36, 2011.

2. D. H. Geschwind and P. Rakic, "Cortical evolution: judge the brain by its cover," *Neuron*, vol. 80, no. 3, pp. 633–647, 2013.

3. Z. Molnár, G. J. Clowry, N. Šestan, A. Alzu'bi, T. Bakken, R. F. Hevner, P. S. Hüppi, I. Kostović, P. Rakic, E. Anton, *et al.*, "New insights into the development of the human cerebral cortex," *J. Anat.*, vol. 235, no. 3, pp. 432–451, 2019.

4. L. Del-Valle-Anton and V. Borrell, "Folding brains: from development to disease modeling," *Physiol. Rev.*, vol. 102, no. 2, pp. 511–550, 2022.

5. S. K. Akula, D. Exposito-Alonso, and C. A. Walsh, "Shaping the brain: The emergence of cortical structure and folding," *Dev. Cell*, vol. 58, no. 24, pp. 2836–2849, 2023.

6. W. Welker, "Why does the cortex fissure and fold: a review of determinants of gyri and sulci," in *Cerebral Cortex (Jones EG, Peters A, eds)*, pp. 3–136, Plenum Press New York, NY, 1990.

7. W. His, *Untersuchungen über die erste Anlage des Wirbelthierleibes: die erste Entwickelung des Hühnchens im Ei*, vol. 1. FCW Vogel, 1868.

8. D. P. Richman, R. M. Stewart, J. W. Hutchinson, and V. S. Caviness, "Mechanical model of brain convolutional development," *Science*, vol. 189, no. 4196, pp. 18–21, 1975.

9. S. A. Fietz, I. Kelava, J. Vogt, M. Wilsch-Bräuninger, D. Stenzel, J. L. Fish, D. Corbeil, A. Riehn, W. Distler, R. Nitsch, *et al.*, "OSVZ progenitors of human and ferret neocortex are epithelial-like and expand by integrin signaling," *Nat. Neurosci.*, vol. 13, no. 6, pp. 690–699, 2010.

10. D. V. Hansen, J. H. Lui, P. R. L. Parker, and A. R. Kriegstein, "Neurogenic radial glia in the outer subventricular zone of human neocortex," *Nature*, vol. 464, no. 7288, pp. 554–561, 2010.

11. V. Borrell, "How cells fold the cerebral cortex," *J. Neurosci.*, vol. 38, no. 4, pp. 776–783, 2018.

12. D. C. Van Essen, "Biomechanical models and mechanisms of cellular morphogenesis and cerebral cortical expansion and folding," in *Seminars in Cell & Developmental Biology*, Elsevier, 2022.

13. E. Hohlfeld and L. Mahadevan, "Unfolding the sulcus," *Phys. Rev. Lett.*, vol. 106, no. 10, p. 105702, 2011.

14. T. Tallinen, J. S. Biggins, and L. Mahadevan, "Surface sulci in squeezed soft solids," *Phys. Rev. Lett.*, vol. 110, no. 2, p. 024302, 2013.

15. T. Tallinen, J. Y. Chung, J. S. Biggins, and L. Mahadevan, "Gyrification from constrained cortical expansion," *Proc. Natl. Acad. Sci.*, vol. 111, no. 35, pp. 12667–12672, 2014.

16. C. D. Kroenke and P. V. Bayly, "How forces fold the cerebral cortex," *J. Neurosci.*, vol. 38, no. 4, pp. 767–775, 2018.

17. T. Tallinen, J. Y. Chung, F. Rousseau, N. Girard, J. Lefèvre, and L. Mahadevan, "On the growth and form of cortical convolutions," *Nat. Phys.*, vol. 12, no. 6, pp. 588–593, 2016.

18. R. Toro and Y. Burnod, "A morphogenetic model for the development of cortical convolutions," *Cereb. Cortex*, vol. 15, no. 12, pp. 1900–1913, 2005.

19. R. Toro, M. Perron, B. Pike, L. Richer, S. Veillette, Z. Pausova, and T. Paus, "Brain size and folding of the human cerebral cortex," *Cereb. Cortex*, vol. 18, no. 10, pp. 2352–2357, 2008.

20. S. Herculano-Houzel, "The human brain in numbers: a linearly scaled-up primate brain," *Front. Hum. Neurosci.*, vol. 3, p. 857, 2009.

21. F. A. C. Azevedo, L. R. B. Carvalho, L. T. Grinberg, J. M. Farfel, R. E. L. Ferretti, R. E. P. Leite, W. J. Filho, R. Lent, and S. Herculano-Houzel, "Equal numbers of neuronal and nonneuronal cells make the human brain an isometrically scaled-up primate brain," *J. Comp. Neurol.*, vol. 513, no. 5, pp. 532–541, 2009.

22. C. Hutton, B. Draganski, J. Ashburner, and N. Weiskopf, “A comparison between voxel-based cortical thickness and voxel-based morphometry in normal aging,” *Neuroimage*, vol. 48, no. 2, pp. 371–380, 2009.

23. J. Nie, L. Guo, G. Li, C. Faraco, L. S. Miller, and T. Liu, “A computational model of cerebral cortex folding,” *J. Theor. Biol.*, vol. 264, no. 2, pp. 467–478, 2010.

24. P. Bayly, R. Okamoto, G. Xu, Y. Shi, and L. Taber, “A cortical folding model incorporating stress-dependent growth explains gyral wavelengths and stress patterns in the developing brain,” *Phys. Biol.*, vol. 10, no. 1, p. 016005, 2013.

25. S. Budday, C. Raybaud, and E. Kuhl, “A mechanical model predicts morphological abnormalities in the developing human brain,” *Sci. Rep.*, vol. 4, p. 5644, 2014.

26. K. E. Garcia, X. Wang, and C. D. Kroenke, “A model of tension-induced fiber growth predicts white matter organization during brain folding,” *Nat. Commun.*, vol. 12, no. 1, p. 6681, 2021.

27. K. Heuer, N. Traut, A. A. de Sousa, S. L. Valk, J. Clavel, and R. Toro, “Diversity and evolution of cerebellar folding in mammals,” *Elife*, vol. 12, p. e85907, 2023.

28. J. C. Pang, K. M. Aquino, M. Oldehinkel, P. A. Robinson, B. D. Fulcher, M. Breakspear, and A. Fornito, “Geometric constraints on human brain function,” *Nature*, vol. 618, no. 7965, pp. 566–574, 2023.

29. E. Schwartz, K.-H. Nenning, K. Heuer, N. Jeffery, O. C. Bertrand, R. Toro, G. Kasprian, D. Prayer, and G. Langs, “Evolution of cortical geometry and its link to function, behaviour and ecology,” *Nat. Commun.*, vol. 14, no. 1, p. 2252, 2023.

30. J. Neal, M. Takahashi, M. Silva, G. Tiao, C. A. Walsh, and V. L. Sheen, "Insights into the gyrification of developing ferret brain by magnetic resonance imaging," *J. Anat.*, vol. 210, no. 1, pp. 66–77, 2007.

31. K. Sawada and M. Watanabe, "Development of cerebral sulci and gyri in ferrets (mustela putorius)," *Congenit. Anom.*, vol. 52, no. 3, pp. 168–175, 2012.

32. M. B. Johnson, X. Sun, A. Kodani, R. Borges-Monroy, K. M. Girskis, S. C. Ryu, P. P. Wang, K. Patel, D. M. Gonzalez, Y. M. Woo, *et al.*, "Aspm knockout ferret reveals an evolutionary mechanism governing cerebral cortical size," *Nature*, vol. 556, no. 7701, pp. 370–375, 2018.

33. C. Gilardi and N. Kalebic, "The ferret as a model system for neocortex development and evolution," *Front. Cell Dev. Biol.*, vol. 9, p. 661759, 2021.

34. K. Masuda, T. Toda, Y. Shinmyo, H. Ebisu, Y. Hoshiba, M. Wakimoto, Y. Ichikawa, and H. Kawasaki, "Pathophysiological analyses of cortical malformation using gyrencephalic mammals," *Sci. Rep.*, vol. 5, no. 1, pp. 1–15, 2015.

35. H. Tabata and K. Nakajima, "Efficient in utero gene transfer system to the developing mouse brain using electroporation: visualization of neuronal migration in the developing cortex," *Neuroscience*, vol. 103, no. 4, pp. 865–872, 2001.

36. T. Tallinen and J. S. Biggins, "Mechanics of invagination and folding: Hybridized instabilities when one soft tissue grows on another," *Phys. Rev. E*, vol. 92, no. 2, p. 022720, 2015.

37. P. T. Choi, K. C. Lam, and L. M. Lui, "FLASH: Fast landmark aligned spherical harmonic parameterization for genus-0 closed brain surfaces," *SIAM J. Imaging Sci.*, vol. 8, no. 1, pp. 67–94, 2015.

38. J. J. Koenderink and A. J. van Doorn, "Surface shape and curvature scales," *Image Vis. Comput.*, vol. 10, no. 8, pp. 557–564, 1992.

39. S. Yin, C. Liu, Y. Jung, G. P. T. Choi, R. Toro, K. Heuer, and L. Mahadevan, "Morphogenesis and morphometry of brain folding patterns across species," *Preprint*, 2025.

40. R. S. Smith, C. J. Kenny, V. Ganesh, A. Jang, R. Borges-Monroy, J. N. Partlow, R. S. Hill, T. Shin, A. Y. Chen, R. N. Doan, *et al.*, "Sodium channel SCN3A (NaV1. 3) regulation of human cerebral cortical folding and oral motor development," *Neuron*, vol. 99, no. 5, pp. 905–913, 2018.

41. S. K. Akula, J. H. Marciano, Y. Lim, D. Exposito-Alonso, N. K. Hylton, G. H. Hwang, J. E. Neil, N. Dominado, R. K. Bunton-Stasyshyn, J. H. T. Song, *et al.*, "TMEM161B regulates cerebral cortical gyration, sonic hedgehog signaling, and ciliary structure in the developing central nervous system," *Proc. Natl. Acad. Sci.*, vol. 120, no. 4, p. e2209964120, 2023.

42. "FIIND: Ferret interactive integrated neuro development atlas." `https://neuroanatomy.github.io/fiind/`, 2018.

43. "NetGen." `https://ngsolve.org/`, 2019.

44. A. Stomakhin, R. Howes, C. Schroeder, and J. M. Teran, "Energetically consistent invertible elasticity," in *Proceedings of the 11th ACM SIGGRAPH/Eurographics conference on Computer Animation*, pp. 25–32, 2012.

45. J. Bonet and A. Burton, "A simple average nodal pressure tetrahedral element for incompressible and nearly incompressible dynamic explicit applications," *Comm. Numer. Meth. Eng.*, vol. 14, no. 5, pp. 437–449, 1998.

46. C. Ericson, *Real-time collision detection*. CRC Press, 2004.

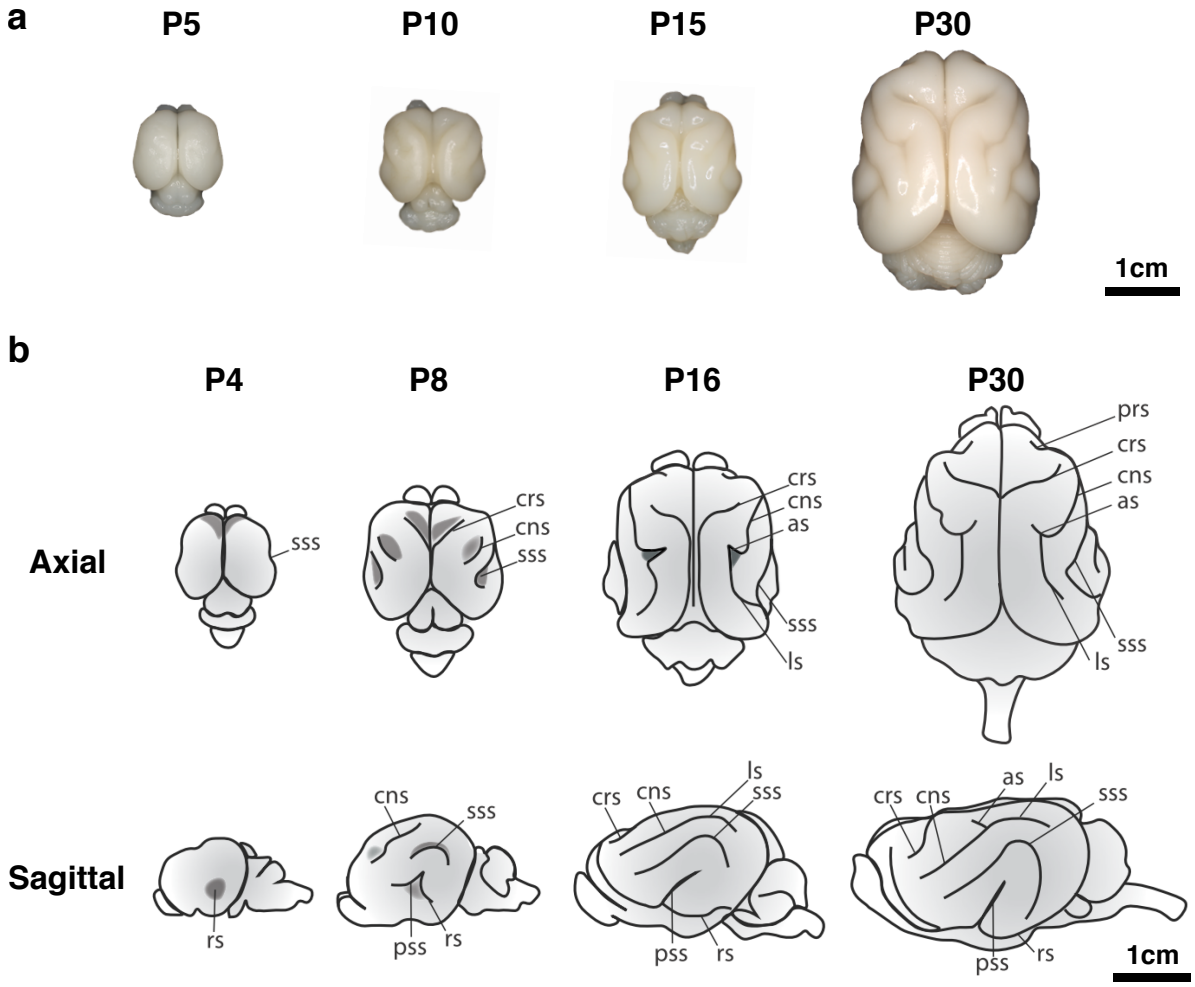

Figure 1: **Time course of ferret brain morphogenesis. a**, Whole brain samples from ferrets of various ages show progressive development of cortical gyri and sulci. **b**, Ferret brains show an increase in complexity of sulcal pattern and in sulcal depth throughout development. The rhinal sulcus (rs), cruciate sulcus (crs), coronal sulcus (cns), suprasylvian sulcus (sss), pseudosylvian sulcus (pss), lateral sulcus (ls), and ansate sulcus (as) are labelled. Schematic by G. Séjourné.

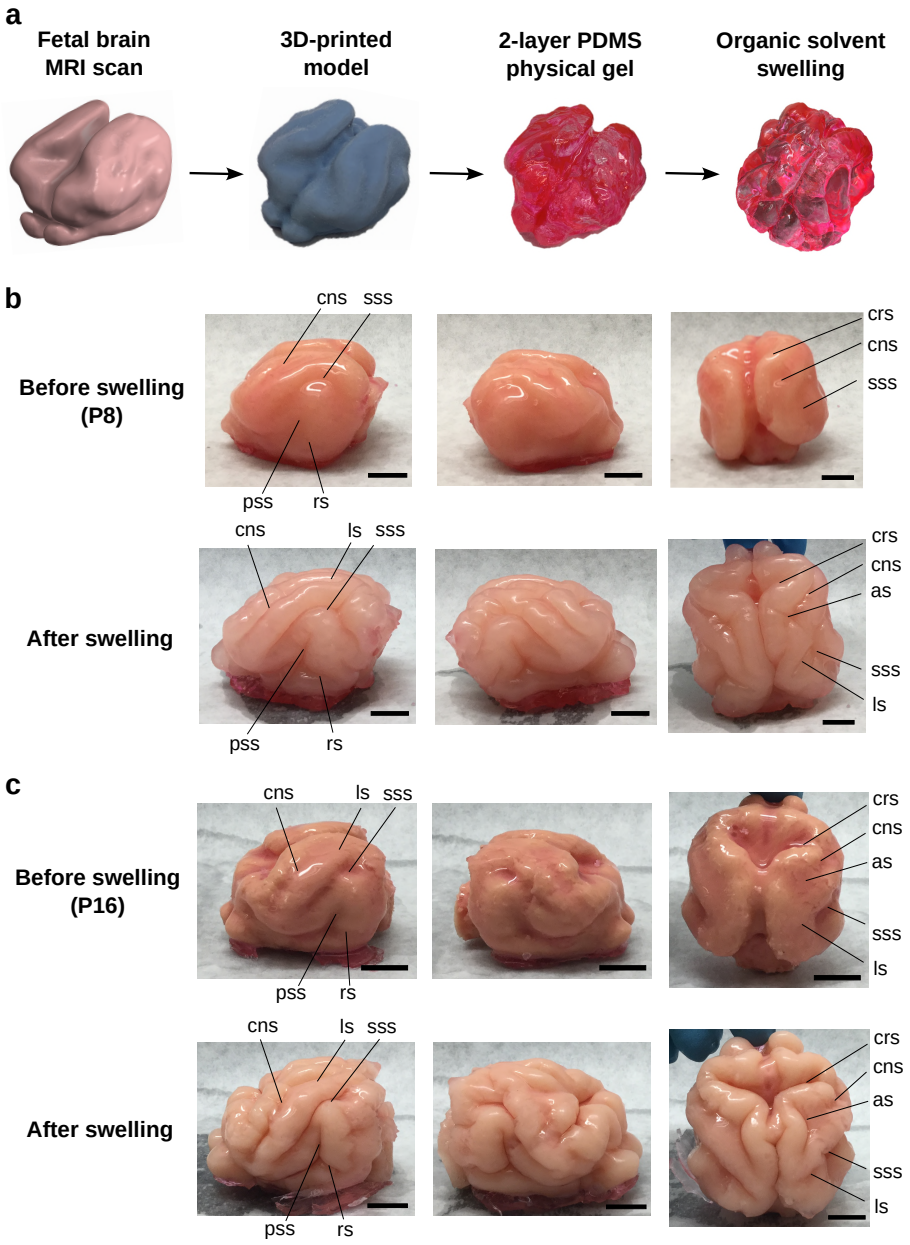

Figure 2: **Physical gel model of ferret brain morphogenesis. a**, Schematic of the gel experiment. We first produced a two-layer gel model of a ferret brain from MRI scans as previously described (*17*). We then immersed the gel model in n-hexane for 1.5 hours, which induced the outer layer to swell by absorbing the solvent over time, resulting in the development of cortical gyri and sulci. **b**, The swelling experiment for the P8 ferret model, in which it can be observed that the swelling of the cortical layer produces sulcal patterns and characteristics comparable to the real ferret brain. **c**, The swelling experiment for the P16 gel model. Scale bar = 1cm. Notation guide: cruciate sulcus (crs), coronal sulcus (cns), suprasylvian sulcus (sss), rhinal sulcus (rs), pseudosylvian sulcus (pss), lateral sulcus (ls), ansate sulcus (as).

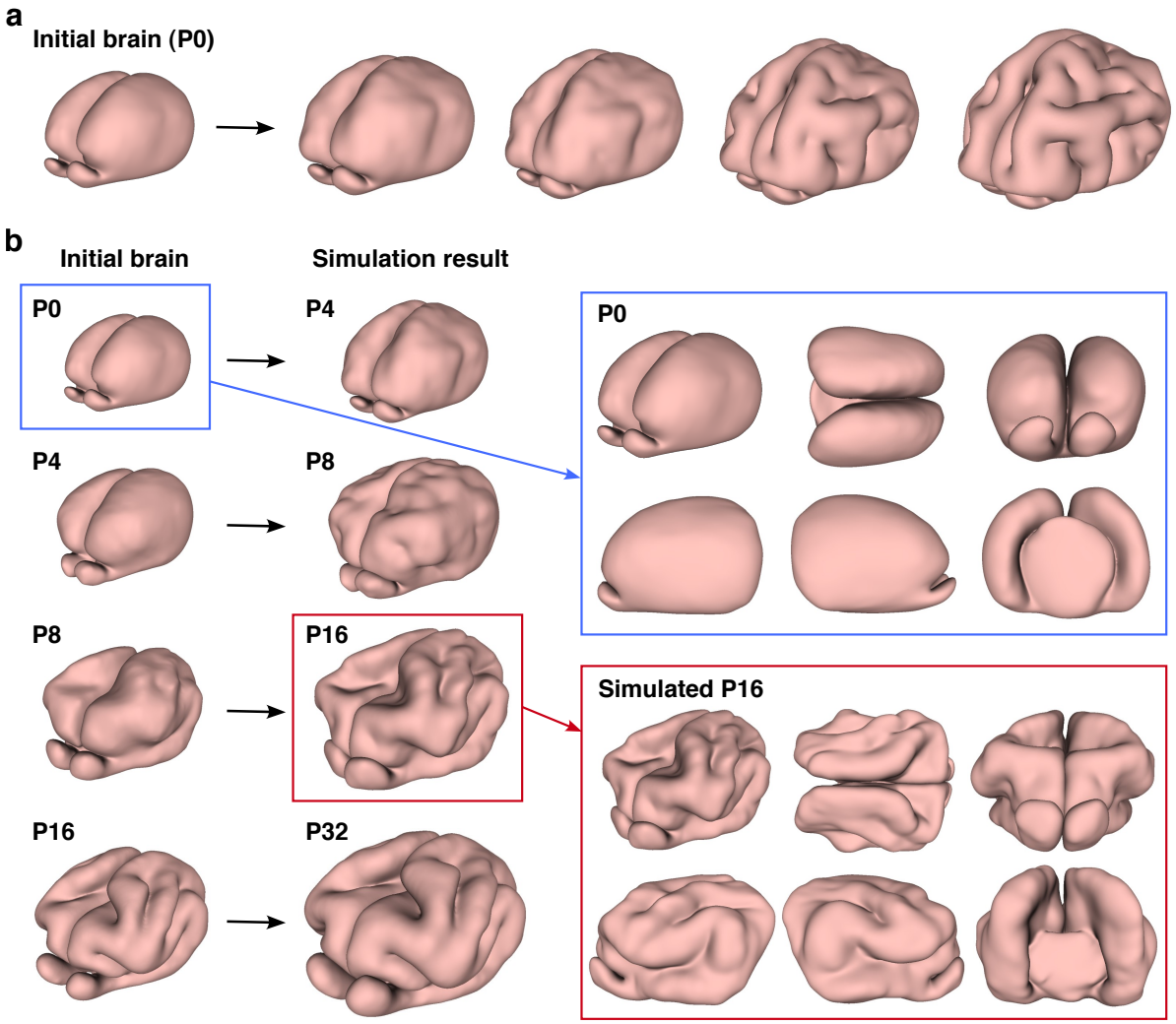

Figure 3: **Numerical model of ferret brain morphogenesis. a**, Continuous growth simulation from P0 to adolescence. The P0 brain tetrahedral mesh was used as the input for the numerical simulation. **b**, Stepwise growth simulation from P0 to P4, P4 to P8, P8 to P16, and P16 to P32. For different growth intervals, we use different brain tetrahedral meshes as the input for the numerical simulation. Different views of the input P0 brain and the simulated P16 brain are provided.

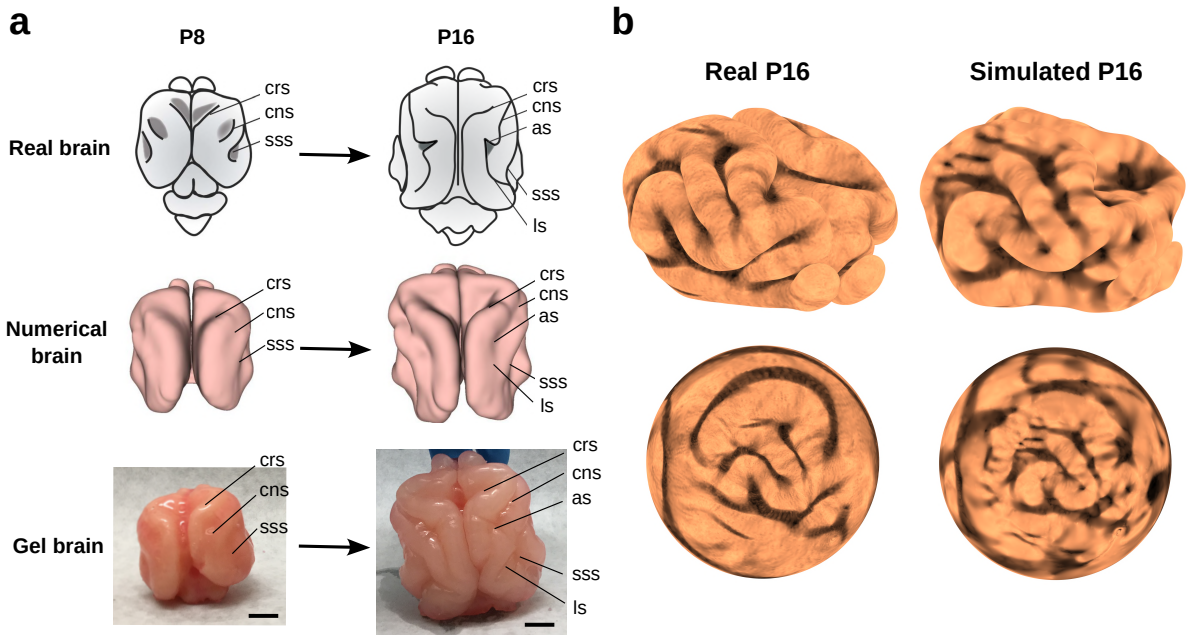

Figure 4: **Comparison of cortical folding in real and simulated ferret brain models. a**, The top row shows the increase in complexity of sulcal pattern and in sulcal depth of ferret brains from P8 to P16. The middle row shows a numerical model of a P8 brain and its deformed state mimicking progression to P16. The bottom row shows a physical gel model of P8 and its post-swelling state mimicking progression to P16 (scale bar = 1cm). The P8 initial states have invaginations corresponding to the cruciate sulcus (crs), coronal sulcus (cns) and suprasylvian sulcus (sss), and both the numerical deformed state and the physical post-swelling state have sulci corresponding in location and self-contacting nature to the crs, cns, sss, lateral sulcus (ls), and ansate sulcus (as) observed in P16 real ferrets. **b**, The real P16 brain reconstructed from MRI scans, the simulated P16 brain, and their respective landmark-aligned spherical mappings obtained by the FLASH algorithm (*37*), each color-coded with the shape index (*38*) of the brain.

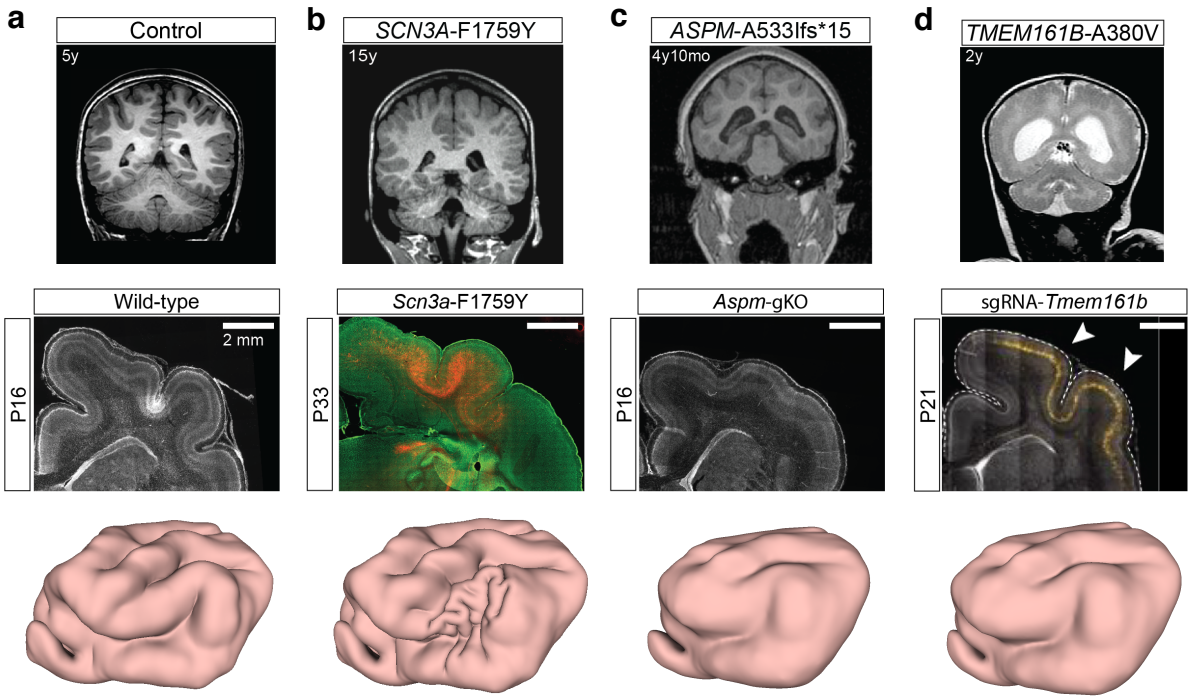

Figure 5: **Modeling malformations of cortical development (MCD) using our model.** **a**, Control. **b**, *SCN3A*. **c**, *ASPM*. **d**, *TMEM161B*. For each example, we show human (top) and ferret (middle) brain MRIs. We then perform a modified numerical brain simulation on the P8 model with different tangential growth rate and cortical thickness parameters, including (**a**) the original growth rate and cortical thickness, (**b**) a reduction of the cortical thickness at a localized zone, (**c**) a reduction of the growth rate globally, and (**d**) a reduction of the growth rate and an increase of the cortical thickness globally. All numerical simulation results (bottom) qualitatively capture the cortical malformations.